vation is confirmed by Fourier analysis of the data. The data clearly demonstrate mode-selective vibrational amplification. The decay of coherent oscillations, measured on an extended time scale, yields a phonon dephasing time of 28.6 ps (*18*). Figure 2C shows ISRS data obtained with the input repetition rate detuned to 2.33 THz (77.8 cm^{-1}). Although the strength of the phonon scattering is reduced, the oscillations are still monochromatic with the same frequency and dephasing rate. Figure 2D shows simulated ISRS data from the repetitively driven 80-cm^{-1} mode, assuming a Gaussian temporal profile for the train of excitation pulses. The numerical results are in good agreement with the data in Fig. 2B.

Multiple-excitation ISRS has also been used to drive the 104-cm^{-1} translational optic phonon mode. The results are shown in Fig. 3. The degree of vibrational amplification achieved for the 104-cm^{-1} mode is comparable to that for the 80-cm^{-1} mode. The intensity of 104-cm^{-1} signal relative to signal from the electronic response is reduced, indicating a smaller differential polarizability for this mode. As with the 80-cm^{-1} mode, slight detuning of the multiple-pulse timing led to a vibrational response with the same frequency and dephasing rate but of weaker amplitude.

We note that femtosecond pulse-shaping technology is still evolving rapidly. Very recently, pulse sequences with square envelopes that would facilitate examination of more heavily damped or inhomogeneously broadened modes have been generated (*16*). Electronically controllable masks based on liquid crystals have been fabricated (*19*) and will allow pulse sequences to be optimized as occasions demand, for example, to drive anharmonic vibrational modes with gradually increased delays between successive pulses. Other electronically controlled pulse-shaping techniques are also moving toward femtosecond time scales (*12*). It is clear that femtosecond pulse shaping will play an important role in optical manipulation of molecular behavior.

REFERENCES AND NOTES

1. R. L. Fork, B. I. Greene, C. V. Shank, *Appl. Phys. Lett.* **38**, 671 (1981).
2. J. A. Valdmanis, R. L. Fork, J. P. Gordon, *Opt. Lett.* **10**, 131 (1985).
3. W. H. Knox, M. C. Downer, R. L. Fork, C. V. Shank, *ibid.* **9**, 552 (1984).
4. R. A. Mathies, C. H. Brito Cruz, W. T. Pollard, C. V. Shank, *Science* **240**, 777 (1988).
5. Y.-X. Yan, L.-T. Cheng, K. A. Nelson, in *Advances in Nonlinear Spectroscopy*, vol. 16 of the *Advances in Spectroscopy Series*, R. J. H. Clark and R. E. Hester, Eds. (Wiley, Chichester, 1988), pp. 299–355; S. Ruhman, A. G. Joly, B. Kohler, L. R. Williams, K. A. Nelson, *Rev. Phys. Appl.* **22**, 1717 (1987).
6. S. De Silvestri *et al.*, *Chem. Phys. Lett.* **116**, 146 (1985).
7. J. Chesnoy and A. Mokhtari, *Phys. Rev. A* **38**, 3566 (1988); F. W. Wise, M. J. Rosker, C. L. Tang, *J. Chem. Phys.* **86**, 2827 (1986); M. Dantus, M. J. Rosker, A. H. Zewail, *ibid.* **89**, 6128 (1988).
8. Y.-X. Yan, E. B. Gamble, Jr., K. A. Nelson, *J. Chem. Phys.* **83**, 5391 (1985); A. G. Joly, S. Ruhman, B. Kohler, K. A. Nelson, in *Ultrafast Phenomena VI*, vol. 48 of the *Springer Series in Chemical Physics*, C. B. Harris and S. Shionoya, Eds. (Springer-Verlag, New York, 1988), pp. 506–510.
9. D. Tannor, R. Kosloff, S. A. Rice, *J. Chem. Phys.* **85**, 5805 (1986); S. Shi, A. Woody, H. Rabitz, *ibid.* **88**, 6870 (1988); B. Hartke, R. Kosloff, S. Ruhman, *Chem. Phys. Lett.* **158**, 238 (1989).
10. C. P. Lin, J. Bates, J. T. Mayer, W. S. Warren, *J. Chem. Phys.* **86**, 3750 (1987).
11. A. M. Weiner, J. P. Heritage, E. M. Kirschner, *J. Opt. Soc. Am. B* **5**, 1563 (1988).
12. M. Haner and W. Warren, *Appl. Phys. Lett.* **52**, 1458 (1988); W. S. Warren, *Science* **242**, 878 (1988).
13. J. Tanaka, T. Kishi, M. Tanaka, *Bull. Chem. Soc. Jpn.* **47**, 2376 (1974); T. Kobayashi, *J. Chem. Phys.* **69**, 3570 (1978).
14. T. J. Kosic, C. L. Schosser, D. D. Dlott, *Chem. Phys. Lett.* **96**, 57 (1983).
15. A. M. Weiner, J. P. Heritage, J. A. Salehi, *Opt. Lett.* **13**, 300 (1988).
16. A. M. Weiner and D. E. Leaird, *ibid.* **15**, 51 (1990).
17. A. M. Weiner *et al.*, *Phys. Rev. Lett.* **61**, 2445 (1988).
18. Note that the homogeneous dephasing rate ultimately limits the number of pulses that can be used for vibrational amplification.
19. A. M. Weiner, D. E. Leaird, J. S. Patel, J. R. Wullert, paper presented at the Optical Society of America Annual Meeting, Orlando, FL, 16 to 20 October 1989.
20. G.P.W. and K.A.N. supported in part by JSEP grant no. DAAL03-89-C-0001.

19 October 1989; accepted 30 January 1990

The Framework Topology of ZSM-18, a Novel Zeolite Containing Rings of Three (Si,Al)-O Species

STEPHEN L. LAWTON* AND WAYNE J. ROHRBAUGH†

ZSM-18 is the first known aluminosilicate zeolite to contain rings of three (Si,Al)-O species (3-rings). Its framework topology has been determined by hypothetical model building, subsequent constrained distance and angle least-squares refinements of atomic coordinates, and x-ray powder diffraction pattern simulations. Its channel structure is characterized by a linear unidimensional 12-ring channel, with an approximate pore opening of 7.0 angstroms. In addition, the channels are lined with pockets that are capped by 7-rings with dimensions of 2.8 angstroms by 3.5 angstroms. An intraframework packing model of the organic moiety used in the synthesis suggests that a strong templating effect may be responsible for the formation of this unusual zeolite structure.

THE ALUMINOSILICATE ZEOLITE ZSM-18, reported by Ciric in 1976 (*1*), is synthesized in the presence of Na^+ and the triply charged tris-quaternary ammonium cation 2,3,4,5,6,7,8,9-octahydro-2,2,5,5,8,8-hexamethyl-1*H*-benzo[1,2-c:3,4-c′:5,6-c″]tripyrrolium (**1**),

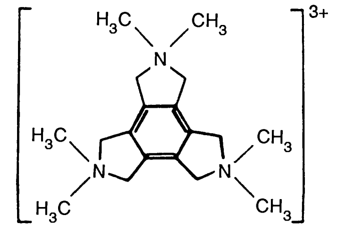

1

hereafter referred to as the triquat cation (*2*, *3*). The synthesis was prompted by the hypothesis that large quaternary ammonium cations may serve as effective templates in the crystallization of zeolites from aluminosilicate gels, which, upon calcination, will leave large pores in the zeolite product. Large-pore zeolites have significant application in petroleum refining and petrochemical processing.

ZSM-18 crystallizes with product ratios of SiO_2 to Al_2O_3 ranging from 10 to 30 (*1*). It has high sorptive capacity for large molecules. For the stable H form, sorptions as high as 23.4% (by weight) for H_2O, 15.0% for *n*-hexane, and 14.7% for cyclohexane have been observed (*1*).

Preliminary studies of ZSM-18 indicated that the unit cell is hexagonal with lattice parameters of a = 13.2 Å and c = 15.8 Å (*1*). The structure was solved when it was recognized that the difference between the c parameter of ZSM-18 (15.8 Å) and one-half the c parameter of the aluminophosphate MAPSO-46 (AFS) framework (13.45 Å) is 2.35 Å (*4*), which is approximately equal to the O · · · O distance in an (Si,Al)O_4 tetrahedron. In considering the AFS framework, it was noted that this particular structure is built entirely out of capped 6-rings. The cap consists of a single T atom (where T is a tetrahedrally coordinated

---

Research Department, Mobil Research and Development Corporation, Paulsboro, NJ 08066.

*To whom correspondence should be addressed.
†Permanent address: Chemical Research and Development Laboratory, ICI Americas, Inc., Wilmington, DE 19897.

atom, either Al or P in this case) bridging three T atoms in the 6-ring through O atoms. Two capped 6-rings, one a mirror image of the other, are joined together through three shared O atoms to form a unit that is capped at both ends (**2** and Fig. 1). Six of these units are then joined together through their edges to form 12-ring channels parallel to the *c* axis.

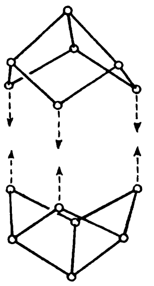

2

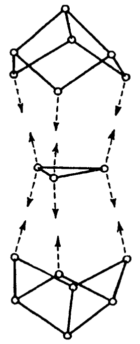

3

When two aluminosilicate 6-ring caps are linked together through a single 3-ring (**3**) instead of to each other through shared O atoms, the length of the doubly capped unit increases from 13.45 to 15.8 Å, which is exactly the *c* parameter in ZSM-18. Two structures, models A and B, can be built with this unit. The symmetries of models A and B are defined by space groups $P\bar{6}2m$ and $P6_3/m$, respectively. We refer to the building unit as the (34^65^6) or (345)-unit, since it is composed of one 3-ring, six 4-rings, and six 5-rings (**3** and Fig. 1) (*5*). The 3-ring is bounded on all sides by 5-rings, which may add stability to the (345)-unit configuration. In both structures, six of the (345)-units link together through their edges to form 12-ring channels parallel to the *c* axis; the unit cell *a* parameter (13.2 Å) remains the same as that of the AFS framework. The two models differ from each other by the absence or presence of translations of the (345)-units along the *c* axis. In model A, no translation is involved; in model B, alternating columns of (345)-units are rotated 60° and then translated one-half the *c* axis (Fig. 1).

A third model, C, with space group symmetry $P\bar{6}2m$, may also be constructed if the single T-atom caps (either Si or Al) above the 6-rings in model A are replaced with 3-rings (Fig. 1). This produces another new unit, designated the (3^25^{12}) or (35)-unit, which is composed of two 3-rings and twelve 5-rings. The secondary building units (SBU) required for model C include the use of the new single 3-ring unit plus a single 6-ring.

All three models were subjected to a constrained distance and angle least-squares (DLS) refinement of atomic coordinates (*6*). In these refinements, the prescribed T–O distance was optimized at 1.61 Å, and the T–O–T bond angle at 145°; the lattice parameters were included in the refinements. Very low *R* and σ values (7), typically 0.008 and 0.05, respectively, were obtained. Comparison of the simulated x-ray diffraction (XRD) powder patterns of these models (*8*) with the observed pattern of the H form of ZSM-18 (H-ZSM-18) demonstrated that model B was the framework structure of ZSM-18.

We indexed the observed XRD powder pattern for H-ZSM-18 by using the known crystallographic indices derived for model B, and the lattice parameters were determined by least-squares refinement with the use of 19 reflections; the refined hexagonal lattice parameters are a = 13.175(3) Å and c = 15.848(6) Å (the number in parentheses is the standard error in the last digit). Model B was then further refined with DLS, but with the lattice parameters fixed at the experi-

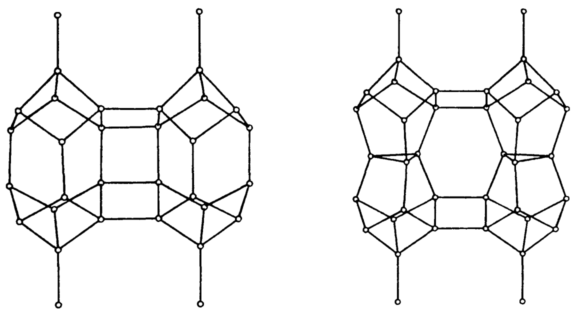

AFS

Model A
Columns of (345)-units

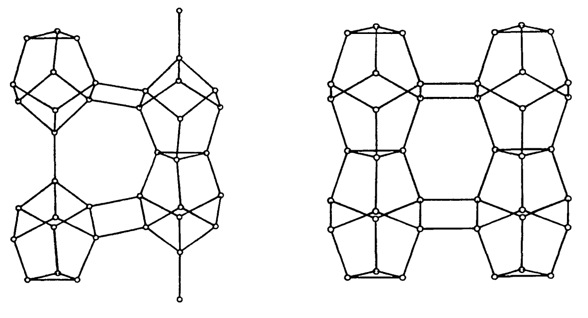

Model B (ZSM-18)
Columns of (345)-units

Model C
Columns of (35)-units

Fig. 1. Comparison of the basic building units in AFS and in models A, B, and C. Crystallographic data for structures in this new 3-ring series are as follows: model A, space group $P\bar{6}2m$ (no. 189), a = 13.08 Å, c = 15.58 Å; model B (ZSM-18), space group $P6_3/m$ (no. 176), a = 13.175(3) Å, c = 15.848(6) Å; and model C, space group $P\bar{6}2m$ (no. 189), a = 13.70 Å, c = 14.12 Å.

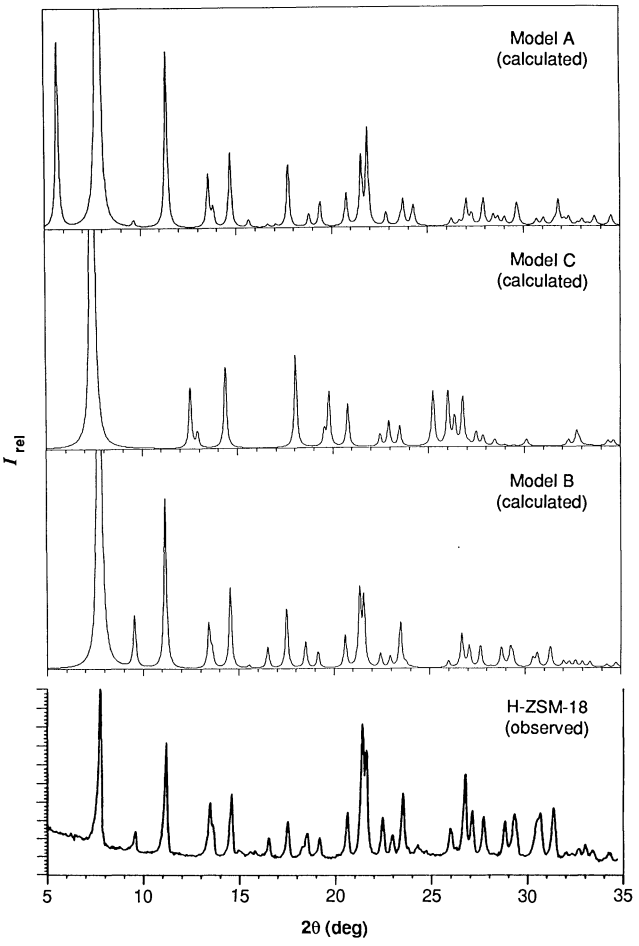

Fig. 2. Comparison of the experimental XRD powder pattern of H-ZSM-18 with the calculated patterns of models A, B, and C.

Table 1. Fractional unit cell coordinates for H-ZSM-18 (model B) (space group: $P6_3/m$, no. 176; $a = 13.175(3)$ Å, $c = 15.848(6)$ Å).

Atom	Position*	x	y	z
T1	4f	0.6667	0.3333	0.3495
T2	12i	0.6713	0.1500	0.4700
T3	12i	0.4522	0.1161	0.5682
T4	6h	0.5266	0.2118	0.75
O1	2d	0.6667	0.3333	0.25
O2	12i	0.6623	0.2169	0.3878
O3	12i	0.5793	0.1388	0.5411
O4	12i	0.4217	0.1984	0.5101
O5	12i	0.4540	0.1495	0.6663
O6	6h	0.6506	0.2126	0.75
O7	12i	0.6443	0.0200	0.4453

*The letters d, f, h, and i correspond to the Wyckoff notations.

mentally determined values for H-ZSM-18. The final R and σ values were 0.0098 and 0.051, respectively.

The DLS-refined atomic coordinates for H-ZSM-18 are presented in Table 1. A comparison of the observed and calculated XRD powder pattern of the H form, based on the final atomic coordinates and unit cell parameters, is shown in Fig. 2. [Diffraction data used in this study were obtained with Cu$K\alpha$ x-rays on a CSS/Nicolet powder diffraction system with a 2θ step size of 0.04° and a 4-s-per-step counting rate (θ is the Bragg angle) (*9*).] Minor intensity differences observed at low diffraction angles are due to the presence of sorbed water in the H form material. The suppression of low-angle diffraction intensities caused by sorbed water in zeolites is well known.

ZSM-18 is, to our knowledge, the first example of an aluminosilicate zeolite containing 3-rings of tetrahedral (Si,Al)-O species. Previously, 3-rings containing Be–O species were observed in a beryllosilicate [lovdarite (*10*)], but 3-rings in aluminosilicate or aluminophosphate materials were unknown. Linking the novel (345)-unit in the *ab* face produces an open 12-ring channel that is lined with pockets. The pockets, which are capped by 7-rings, can be accessed from the open channel through 12-ring apertures (Fig. 3). The threefold symmetry produced by the linking of the (345)-units does not permit stacking faults to occur, and thus the channel cannot be blocked by framework material.

Despite the unusual structural features (3-rings and 7-rings), DLS refinement of the structure was straightforward and converged to very low R and σ values (see above). The T–O bond distances ranged from 1.58 to 1.63 Å, and non–symmetry-constrained T–O–T bond angles ranged from 135° to 151°. As might be predicted, the smallest T–O–T angles (135°) involved atoms within the 3-rings, but the deviation from an "ideal" T–O–T angle was only about 10°. Oxygen atoms constrained by the threefold axis during the DLS treatment, with a linear T–O–T angle (180°), represent an average structure describing an infinite set of displaced O atom positions with varying occupancies. Thus, the 180° bond angle about O1 is a manifestation of the symmetry constraint of the average structure described here and should not be viewed as an actual linear T–O–T linkage.

Although the three-dimensional structure has only threefold symmetry ($\bar{6}$), in projection the *ab* face displays a sixfold axis. The 12-ring channel has a nearly circular pore opening with dimensions of 6.9 Å by 7.0 Å, and so it is slightly larger than mordenite (6.5 Å by 7.0 Å) but smaller than faujasite (7.4 Å by 7.4 Å). (Pore size calculations assume an O^{2-} radius of 1.35 Å.) In addition, ZSM-18 has a 7-ring "channel" that is perpendicular to the 12-ring channel. Its aperture has minimum and maximum openings of 2.8 and 3.5 Å, respectively. As found for other zeolite pore systems, the effective pore size of this 7-ring channel can be estimated to be nearly 1 Å larger than the crystallographically determined value (*11*), thus potentially permitting diffusion of small normal paraffins and olefins. [For example, the kinetic diameters for CH_4, C_2H_4, and n-C_4H_{10} are 3.8, 3.9, and 4.3 Å, respectively (*12*).]

The framework density (FD), the number of tetrahedral (Si,Al) atoms per 1000 Å^3, is 14.3, which is slightly greater than for the zeolites faujasite and Linde type A (12.7 and 12.9, respectively) but significantly less than for mordenite and ZSM-5 (17.2 and 17.9, respectively) (*10*). The FD of ZSM-18 is consistent with the tabulation by Brunner and Meier (*13*), which demonstrates that the frameworks of lowest FD are those with a maximum number of very small rings (such as 3- or 4-rings, or both) per T atom.

One can explore the role of the triquat

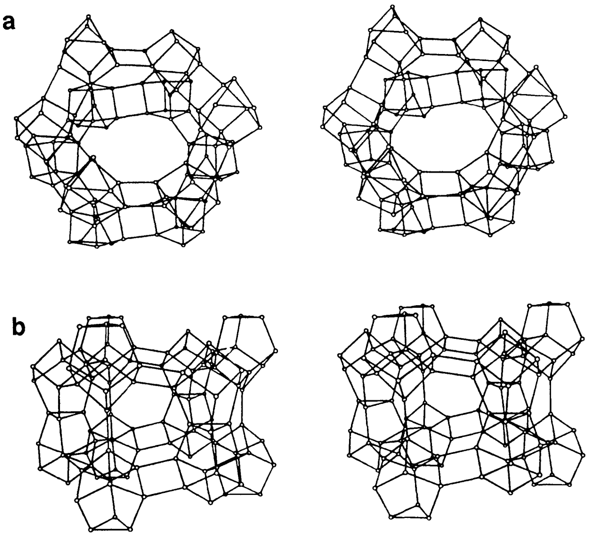

Fig. 3. Stereo views of the ZSM-18 framework (model B). (**a**) Top view through the 12-ring. (**b**) Side view through 7-rings.

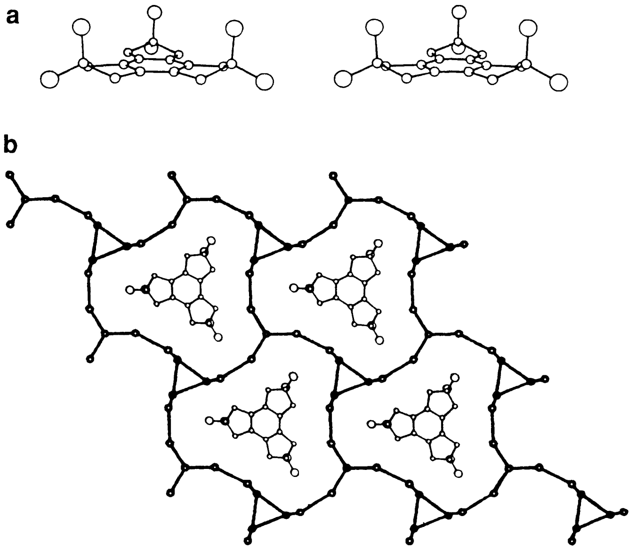

Fig. 4. Illustration of the influence of the triquat cation as a template on the formation of the ZSM-18 framework. (**a**) Stereo view of the triquat cation (*3*); (H atoms are omitted). (**b**) Outline of the (Si,Al) framework between $z = 0$ and $z = 1/2$, as viewed along the [001] unit cell direction. The proposed locations of the triply positive triquat cations relative to the 3-rings in the framework are shown. (The cations are drawn to the same scale as the framework.)

cation as a template by examining the interior volume defined by the channel and pocket features of the ZSM-18 structure. A slice of the unit cell between $z = 0$ and $z = 1/2$ can be viewed along the c axis to outline the largest interior volume projection. Since the structure of the triquat cation is known (*2*, *3*), it can be drawn to scale within that volume. A stereo drawing of the triquat cation and the proposed locations of the triply charged ions within the ZSM-18 structure are shown in Fig. 4. The scaled projection drawing shows that the triquat moiety must occupy rather specific positions within the framework structure of ZSM-18. The probable arrangements of aluminosilicate anions and organic cations that would favor cocrystallization make it less surprising that a 3-ring of aluminosilicate material could form to balance the positively charged triquat. Clearly, this suggests, however, that the formation of ZSM-18 and perhaps any 3-ring aluminosilicate zeolite may depend on the judicious choice of a bulky, multiply charged, cationic templating species.

REFERENCES AND NOTES

1. J. Ciric, U.S. Patent 3,950,496 (1976).
2. ———, S. L. Lawton, G. T. Kokotailo, G. W. Griffin, *J. Am. Chem. Soc.* **100**, 2173 (1978).
3. S. L. Lawton, J. Ciric, G. T. Kokotailo, *Acta Crystallogr. Sect. C* **41**, 1683 (1985).
4. J. M. Bennett and B. K. Marcus, in *Innovation in Zeolite Materials Science*, P. J. Grobet, W. J. Mortier, E. F. Vansant, G. Schulz-Ekloff, Eds. (Elsevier, Amsterdam, 1988), vol. 37, pp. 269–279. MAPSO-46 is an aluminophosphate with the composition $Mg_6Al_{22}P_{26}Si_2O_{112}$ (Mg is an extra framework cation, and the locations of the Si impurity atoms are unknown).
5. The International Zeolite Association designation for secondary building units (SBU) for these structures requires the introduction of a new SBU, the single 3-ring, in order to describe them. For models A and B, the SBU requirements are a single 3-ring + 6≡1, where the symbol 6≡1 refers to a capped 6-ring.
6. C. Baerlocher, A. Hepp, W. M. Meier, Program DLS-76 (Eidgenössische Technische Hochschule, Zurich, revised March 1978; in-house modifications, November 1981).
7. The weighted agreement values R and σ are computed as follows (*6*):

$$R_w = \left\{ \sum_{\substack{j \\ (m,n)}} [w_j(D_j^\circ - D_j^{m,n})]^2 / \sum_j (w_j D_j^\circ)^2 \right\}^{1/2}$$

$$\sigma = \left\{ \sum_{\substack{j \\ (m,n)}} [w_j(D_j^\circ - D_j^{m,n})]^2 / (M - NV) \right\}^{1/2}$$

where w_j are the weights associated with each interatomic distance type j between atoms m and n ($D_j^{m,n}$) (such as T–O, T–T, and O–O), M is the number of distances, and NV is the number of variables. D_j° are the prescribed distances for each type and are determined by:

$$D^\circ = A + B(\mathrm{TOT} - \omega) + C(\mathrm{TOT} - \omega)^2 + \ldots,$$

where A, B, and C are constants, TOT is the calculated angle about each O, and ω is the standard T–O–T angle, for example, 145°. In our calculations, $A = 1.61$, $B = -4 \times 10^{-4}$, and $C = \mathrm{O}$.
8. D. K. Smith, M. C. Nichols, M. E. Zolensky, Program POWD10 (College of Earth and Mineral Sciences, Pennsylvania State University, University Park, PA, March 1983).
9. Synchrotron XRD powder data of the hydrated, uncalcined form of ZSM-18 have also been obtained; refinement of the framework and cation with the use of the Rietveld procedure is in progress.
10. W. M. Meier and D. H. Olson, *Atlas of Zeolite Structure Types* (Butterworths, London, ed. 2, 1987).
11. A. W. Chester, P. Chu, W. J. Rohrbaugh, paper presented at the North American Catalysis Society meeting, San Diego, CA, May 1987.
12. D. W. Breck, *Zeolite Molecular Sieves* (Wiley, New York, 1974), p. 636.
13. G. O. Brunner and W. M. Meier, *Nature* **387**, 146 (1989).
14. Dedicated to Julius Ciric, deceased.

16 October 1989; accepted 18 January 1990

Amazon Deforestation and Climate Change

J. SHUKLA, C. NOBRE,* P. SELLERS

A coupled numerical model of the global atmosphere and biosphere has been used to assess the effects of Amazon deforestation on the regional and global climate. When the tropical forests in the model were replaced by degraded grass (pasture), there was a significant increase in surface temperature and a decrease in evapotranspiration and precipitation over Amazonia. In the simulation, the length of the dry season also increased; such an increase could make reestablishment of the tropical forests after massive deforestation particularly difficult.

THE DISTRIBUTION OF GLOBAL VEGETATION was traditionally thought to be determined by local climate factors, especially precipitation and radiation. This view has been modified because controlled numerical experiments with complex models of the atmosphere showed that the presence or absence of vegetation can influence the regional climate (*1–3*). One implication of these results is that the current climate and vegetation may coexist in a dynamic equilibrium that could be altered by large perturbations in either of the two components. The high rate of deforestation in the Brazilian portion of Amazonia, from 25,000 to 50,000 km^2 per year (*4–7*), might thus be expected to have an effect on the regional climate. If deforestation were to continue at this rate, most of the Amazonian tropical forests would disappear in 50 to 100 years.

Removal of the Amazonian forest would also have tremendous effects on species diversity and atmospheric chemistry (*8*). The Amazon basin is host to roughly half of the world's species, and the intensity and complexity of plant-animal interactions (*9*) and the rapid nutrient cycling in the soils (*10*) make the region vulnerable to external disturbances. The Amazon is also an important natural sink for ozone and plays an important role in global tropospheric chemistry. The present study is mainly confined to the assessment of the effects of deforestation on the physical climate system.

Quantitatively estimating the effects that large changes in terrestrial ecosystems can have on temperature, circulation, and rainfall has been difficult because the equilibrium climate is determined by complex interactions among the dynamical processes in the atmosphere and thermodynamic processes at the earth-atmosphere interface. Realistic models of the biosphere that can be coupled with realistic models of the global atmosphere have only recently been developed (*11*, *12*). In this report, we describe the use of a coupled atmosphere-biosphere model (*13*, *14*) to investigate the consequences of the removal of Amazon forests on climate.

In the simulations, we assumed that the

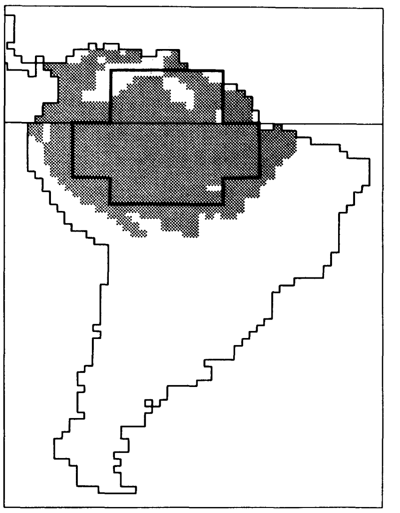

Fig. 1. The South American region. Stippling depicts the area covered by the tropical forest in the control simulation. The area marked with bold lines was used for the areal averages of Fig. 3 and for Tables 1 and 2.

Center for Ocean-Land-Atmosphere Interactions, Department of Meteorology, University of Maryland, College Park, MD 20742.

*Permanent affiliation: Instituto de Pesquisas Espaciais, 12201 Sao Jose dos Campos, SP, Brazil.